# Suppression of the release of arsenic from arsenopyrite by carrier-microencapsulation using Ti-catechol complex

**Ilhwan Park[a, †, *], Carlito Baltazar Tabelin[b, †], Kagehiro Magaribuchi[a], Kensuke Seno[a], Mayumi Ito[b], Naoki Hiroyoshi[b]**

[a] Laboratory of Mineral Processing and Resources Recycling, Division of Sustainable Resources Engineering, Graduate School of Engineering, Hokkaido University, JAPAN

[b] Laboratory of Mineral Processing and Resources Recycling, Division of Sustainable Resources Engineering, Faculty of Engineering, Hokkaido University, JAPAN

[†]These authors contributed equally to this work

* Corresponding author at: Division of Sustainable Resources Engineering, Graduate School of Engineering, Hokkaido University, Kita 13, Nishi 8, Kita-ku, Sapporo 060-8628, Hokkaido, JAPAN.

E-mail address: ihp2035@gmail.com (Ilhwan Park)

## GRAPHICAL ABSTRACT

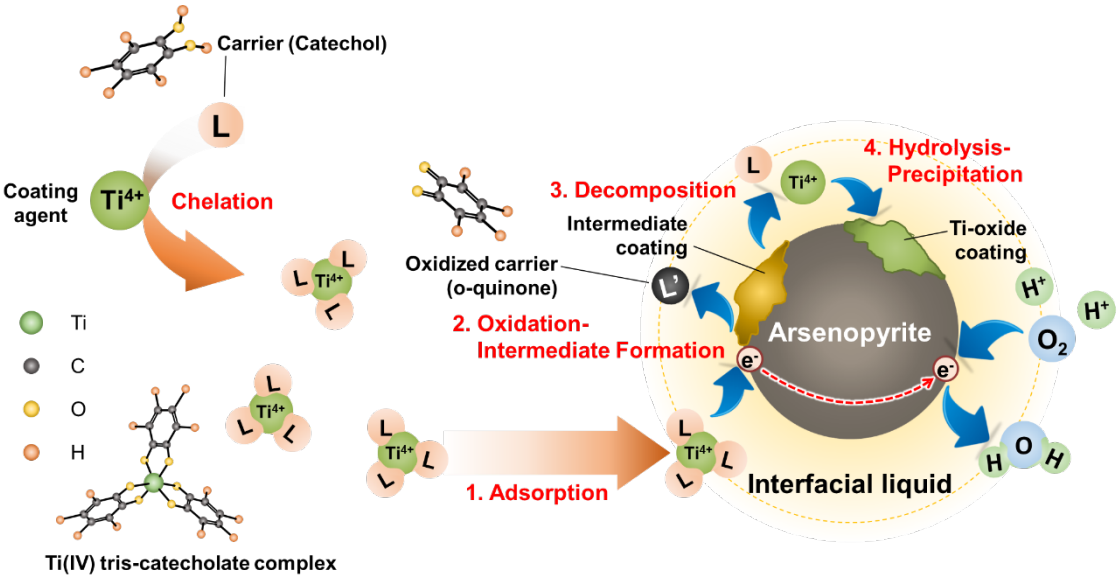


## HIGHLIGHTS

• Ti(IV) Tris-catecholate complex was synthesized between pH 5 and 12.

• Ti-based CME limited the release of As from arsenopyrite.

• Mechanism of CME involved adsorption, oxidation, dissociation and coating formation.

• Ti-oxide coating was formed on arsenopyrite.

## ABSTRACT

Arsenopyrite is the most common arsenic-bearing sulfide mineral in nature, and its weathering contributes to acid mine drainage (AMD) formation and the release of toxic

arsenic (As). To mitigate this problem, carrier-microencapsulation (CME) using titanium (Ti)-catechol complex (i.e., Ti-based CME) was investigated to passivate arsenopyrite by forming a protective coating.

$Ti^{4+}$ ion dissolved in sulfuric acid and catechol were used to successfully synthesize Ti(IV) tris-catecholate complex, $[Ti(Cat)_3]^{2-}$, which was stable in the pH range of 5–12. Electrochemical studies on the redox properties of this complex indicate that its oxidative decomposition was a one-step, irreversible process. The leaching of As from arsenopyrite was suppressed by CME treatment using the synthesized Ti-catechol complex. Scanning electron microscopy with energy dispersive X-ray spectroscopy (SEM-EDX) and diffuse reflectance infrared Fourier transform spectroscopy (DRIFTS) indicate that this suppression was primarily due to the formation of an anatase ($\beta$-$TiO_2$)-containing coating. Based on these results, a detailed 4-step mechanism to explain the decomposition of $[Ti(Cat)_3]^{2-}$ and formation of $TiO_2$ coating in Ti-based CME is proposed: (1) adsorption, (2) partial oxidation-intermediate formation, (3) non electrochemical dissociation, and (4) hydrolysis-precipitation.

***Keywords:*** Acid mine drainage, Arsenic, Arsenopyrite, Microencapsulation, Ti-catechol complex

## 1. Introduction

Mining, mineral processing and tunnel/underground construction for roads and railways often generate large amounts of wastes that contain sulfide minerals such as pyrite ($FeS_2$) and arsenopyrite (FeAsS), which produce acid mine drainage (AMD) when exposed to the environment [1–14]. AMD is very acidic and could further extract heavy metals (e.g., Fe, Cu, Zn, and Pb) from other minerals found in the wastes. Because of this, AMD could cause serious environmental problems if left untreated [15–18].

Many techniques have been proposed to prevent the oxidation of sulfide minerals, the majority of which relied on limiting the exposure of sulfidic wastes to oxygenated water. One example is microencapsulation, a technique wherein pyrite is coated with oxidatively stable materials to prevent the reaction of this mineral to water and oxygen [19,20]. In one of the microencapsulation techniques introduced by Evangelou [19], hydrogen peroxide ($H_2O_2$) was used to oxidize ferrous ion ($Fe^{2+}$), one of the products of pyrite oxidation, to ferric ion ($Fe^{3+}$) to form insoluble ferric phosphate on pyrite, which could act as a protective coating against further oxidation. Pyrite oxidation was effectively suppressed by this technique, but if used haphazardly, it may cause eutrophication of the receiving water bodies because of excess phosphate [2]. Moreover,

$H_2O_2$ could not specifically target pyrite in real wastes leading to unnecessarily large consumption of expensive reagents.

A great improvement to this technique that addressed these two limitations was proposed by Satur et al. [21] called carrier-microencapsulation (CME). CME uses a redox-sensitive organic compound to carry and deliver the coating material, usually an insoluble metal(loid) ion, preferentially to the surface of pyrite where it is adsorbed or precipitated to form the protective coating. Phosphate is not needed in CME, so the risk of causing eutrophication due to excessive phosphate use is eliminated. Moreover, the redox-sensitive complex used in CME could specifically target pyrite and arsenopyrite because their dissolution is electrochemical in nature [25], a process that requires movement of electrons between distinct anodic and cathodic sites. Because CME could target pyrite and arsenopyrite even in complex systems containing other minerals like silicates and aluminosilicates, unwanted consumption of chemicals during treatment is dramatically reduced. This technique has been shown to suppress pyrite oxidation as well as pyrite floatability in coal flotation [21–24].

In the first CME study of Satur et al. [21], titanium (Ti)-catechol complex was synthesized by mixing $TiO_2$ minerals (rutile and anatase) and pyrocatechol (1,2-dihydroxybenzene). These authors showed that although catechol could extract

Ti-ions from $TiO_2$ directly, extraction efficiency was very low. CME was also successfully applied to suppress pyrite oxidation in this previous study but the mechanism(s) involved remained unclear because the authors mixed $TiO_2$ and catechol together with pyrite. In other words, suppression of pyrite oxidation by Ti-catechol complex was masked by the effects of $TiO_2$ and "free" catechol. Mineral oxides attached to pyrite could directly minimize its oxidation by protecting cathodic sites from oxidants like dissolved $O_2$ (DO) and $Fe^{3+}$[26,27]. Likewise, free catechol might indirectly suppress pyrite oxidation by consuming DO and forming stable complexes with $Fe^{3+}$[28,29]. The electrochemical properties of free catechol and Ti-catechol complex was also not elucidated in detail by this previous research, so the mechanism involved in Ti-catechol complex formation and oxidative decomposition remains poorly understood.

In this study, we investigated the effects of pH and molar ratio on the formation of Ti-catechol complex, and developed a simple and more efficient method to synthesize it for CME treatment. Electrochemical studies (i.e., cyclic voltammetry and chronoamperometry) were carried out to understand the electrochemical behavior of synthesized Ti-catechol complex and identify the mechanism(s) involved in its oxidative decomposition as well as in its ability to passivate arsenopyrite. Finally, the

synthesized Ti-catechol complex was used to treat arsenopyrite (FeAsS), the most common arsenic-bearing sulfide mineral closely associated with gold and copper mineralization [30–34]. Arsenopyrite was selected because not only is it common in mine wastes but its weathering also leads to the release of toxic arsenic (As) into the environment. Arsenic is a strictly regulated contaminant because of its serious negative human health effects even at very low concentrations (i.e., μg/L levels) [30,35–38].

## 2. Materials and methods

### *2.1. Ti-catechol complex synthesis and characterization*

#### *2.1.1. Synthesis method*

In our preparation method to synthesize Ti-catechol complex, $Ti^{4+}$ ions and catechol molecules were mixed directly at very acidic condition (pH < 2). Several studies have already reported that Ti-oxides (i.e., rutile, anatase and ilmenite) dissolve in concentrated sulfuric acid solutions [39–41], so we skipped the dissolution part in this study. Instead, Ti-catechol complex was prepared by mixing reagent grade pyrocatechol and in place of $TiO_2$ dissolved in concentrated $H_2SO_4$, we used high purity (99.9%) titanium solution ($Ti^{4+}$ in 1 M $H_2SO_4$) (Wako Chemical Co. Ltd., Japan) to avoid the effects of contaminants like Si and Fe that are ubiquitous in $TiO_2$ ores.

Our preliminary experiments showed that Ti-catechol complex was only synthesized when the very acidic $Ti^{4+}$ and catechol mixture was rapidly neutralized between pH 5 −12. If neutralization was more gradual (e.g., titration), Ti-catechol complex was not formed because $Ti^{4+}$ ions were rapidly precipitated to $TiO_2$. In the succeeding sections, all Ti-catechol solutions were prepared by “rapid neutralization”.

*2.1.2. Ti-complex formation with various stoichiometric molar ratios of $Ti^{4+}$ to catechol*

Catechol is a strong chelating agent that coordinates with various metal ions (e.g., $Ti^{4+}$, $Fe^{3+}$, $Cu^{2+}$, and etc.) to form several metal-catechol complexes (i.e., mono-, bis- and tris-catecholate) [42,43]. To evaluate the composition of Ti-catechol complex(es) formed during synthesis, 1 mM of $Ti^{4+}$ solution was mixed with catechol at varying stoichiometric molar ratios of $Ti^{4+}$ to catechol (1:0-1:5) (25 °C and 200 rpm). The pH of each solution was then rapidly adjusted to 9, and transferred to a volumetric flask for final volume adjustment. The solutions were then filtered through 0.2 μm syringe-driven filters (Sartorius AG, Germany) and analyzed by an inductively coupled plasma atomic emission spectrometer (ICP-AES, ICPE 9820, Shimadzu Corporation, Japan).

*2.1.3. Identification of Ti-catechol complex stability*

Solutions containing $Ti^{4+}$ only (1 mM $Ti^{4+}$) and 1:3 molar ratio of $Ti^{4+}$ to catechol (1 mM $Ti^{4+}$ and 3 mM catechol) were prepared at pH values ranging from 0 to 12 to

evaluate the formation and stability of Ti-catechol complex. After rapid neutralization and equilibration, the pH were measured and filtrates were collected by filtration to remove precipitates and polymerized organic molecules prior to ICP-AES analyses.

*2.1.4. Ultraviolet-visible light spectrophotometric measurements*

Ultraviolet-visible light (UV–vis) spectrophotometric measurements (UV-2500 PC, Shimadzu Corporation, Japan) were conducted to identify Ti-catechol complex(es) formed under various conditions. Catechol only and Ti-catechol solutions adjusted to various pH (1, 3, 6 and 9) were measured in a single-crystal quartz cell between 250 and 550 nm.

*2.2. Electrochemical studies*

Cyclic voltammetry (CV) measurements were performed using SI 1280 B electrochemical measurement unit (Solartron Instruments, UK) with a conventional three-electrode system (Supplementary information, Fig. S1). Platinum (Pt) electrode, platinum wire and Ag/AgCl electrode filled with 3.3 M NaCl were used as working, counter and reference electrodes, respectively. Three types of solutions were measured by CV: 6 mM catechol at pH 5, 6 mM catechol at pH 9 and Ti-catechol solution (2 mM $Ti^{4+}$ and 6 mM catechol) at pH 9, all of which were prepared in 0.1 M $Na_2SO_4$ as supporting electrolyte. All experiments were carried out at 25 °C under nitrogen

atmosphere. The CV measurements started after equilibration at the open circuit potential (OCP), and the sweep direction was towards more positive potentials first (i.e., anodic direction) at a scan rate of 5 mV/s for 5 cycles. In addition, CV measurements of Ti-catechol solution (pH 9) at various scan rates of 1, 5 and 30 mV/s were carried out.

Chronoamperometry was performed to identify the products formed when Ti-catechol complex is anodically decomposed. In this experiment, a setup similar to the CV measurements was used but with magnetic stirring at 200 rpm. The Ti-catechol complex solution was first equilibrated at the OCP, and then anodically polarized at +1.0 V vs. SHE for 3 h. After this, the Pt working electrode was analyzed by scanning electron microscopy with energy dispersive X-ray spectroscopy (SEM-EDX, SSX-550, Shimadzu Corporation, Japan) to determine the oxidation products deposited on it.

*2.3. Batch leaching experiments*

Three types of solutions were used as leachants in the batch leaching experiments: deionized (DI) water (18 MΩ cm, Milli-Q® Integral Purification System, Merck Millipore, USA) (control), catechol (15 mM catechol), and synthesized Ti-catechol complex (5 mM $Ti^{4+}$ and 15 mM catechol), all of which were adjusted to pH 9 before mixing them with washed arsenopyrite. The washing technique used to remove any oxidized layer formed on arsenopyrite during sample preparation was based on the

method developed by McKibben et al. [44]. This method involves ultrasonic desliming in methanol, washing with 1.8 M $HNO_3$, rinsing with DI water, dewatering with acetone, and drying in a vacuum desiccator. For the leaching experiments, 1 g of arsenopyrite and 10 ml of prepared leachant were put in a 50 ml Erlenmeyer flask and shaken in a constant temperature water bath (25 °C) at 120 strokes/min under oxic conditions for up to 25 days. All leaching experiments were done in triplicates to ascertain that differences observed were statistically significant. At pre-designated time intervals, samples were collected, and their pH and oxidation-reduction potential (Eh) were measured. The leachates were collected by filtration through 0.2 μm syringe-driven membrane filters, and immediately analyzed using ICP-AES to measure the concentrations of As and Ti. Meanwhile, the residues were thoroughly washed with DI water and vacuum-dried at 40 °C for 24 h. After drying, the residues were analyzed by SEM-EDX to observe the surface of leached arsenopyrite. In addition, diffuse reflectance infrared Fourier transform spectroscopy (DRIFTS, FT/IR-6200HFV with DR PR0410-M attachment, Jasco Analytical Instruments, USA) was used to characterize changes in the surface of samples before and after leaching under the following conditions: 1000 scans at a resolution of 4 $cm^{-1}$ and in the range of 400–4000 $cm^{-1}$.

## 3. Results and discussion

*3.1. Evaluation and characterization of Ti-catechol complex*

The effects of pH and solution composition on Ti-catechol complex formation and stability are illustrated in Fig. 1. In the absence of catechol, $Ti^{4+}$ ions remained dissolved in solution under strongly acidic conditions (less than pH 2.0) (Fig. 1a). At pH values higher than 3.5, whitish colored particulates were observed and the concentration of $Ti^{4+}$ ions decreased below the detection limit of ICP-AES (0.001 mg/L), which could be attributed to precipitation of $Ti^{4+}$ as titanium oxide (TiO2). This deduction is supported by thermodynamic considerations as illustrated by the equilibrium log activity-pH diagram of $Ti(OH)_4$ at 25 °C (Fig. 1b), which show that the stability of $Ti^{4+}$ as the hydrolyzed $Ti(OH)_4$ ion decreases with pH from 0 to 4. With catechol, however, the solubility of $Ti^{4+}$ ion dramatically increased and the plot exhibited three distinct regions (Fig. 1a). Regions I and II have similar trends with those of the $Ti^{4+}$ only solution, indicating that $Ti^{4+}$ ions in Region I exist because of the very acidic pH while the rapid $Ti^{4+}$ concentration decrease in Region II was due primarily to the precipitation of $TiO_2$. In Region III, $Ti^{4+}$ concentration started increasing after pH 3.5 coincident with the change in color of solution from transparent to light orange, both of which are strong

indicators of Ti-catechol complex formation [42]. Over 80% of $Ti^{4+}$ ion remained in aqueous phase above pH 5.5 (Region III), indicating that most of it was complexed with catechol because $Ti^{4+}$ ion alone cannot exist in solution at this pH without any complexation reaction (Fig. 1a and b).

To identify the composition of synthesized Ti-catechol complex, solutions of $Ti^{4+}$ and catechol with various molar ratios at pH 9 were investigated. As shown in Fig. 1c, $Ti^{4+}$ concentration increased at higher molar ratios of catechol to $Ti^{4+}$ until the catechol/$Ti^{4+}$ ratio reached 3. These results fitted well with the theoretical curve of $Ti^{4+}$ ion coordinated with three catechol molecules in the tris-catecholate configuration, suggesting that the synthesized Ti-catechol complex was most likely $[Ti(Cat)_3]^{2-}$. The complexation reaction of $Ti^{4+}$ and catechol could be explained as follows:

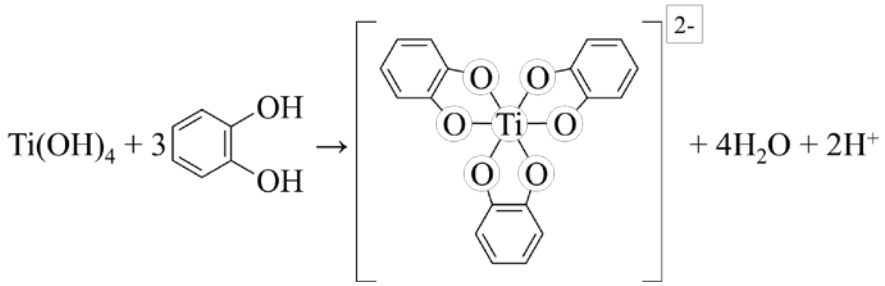


(1)

This deduction is also supported by UV–vis spectrophotometric measurements of "free" catechol and Ti-catechol solutions at pH 1, 3, 6 and 9 (Fig. 1d). Solutions of $Ti^{4+}$ and catechol at pH 1 and 3 showed only one absorption peak at 274 nm, but at pH 6 and 9, a new peak appeared at around 382 nm. The absorption peak at 274 nm could be

attributed to catechol as suggested by the UV–vis spectra of “free” catechol under various pH conditions (Fig. 1d) while the broad absorption band between 375 and 389 nm is assigned to the Ti(IV) tris-catecholate complex consistent with the results of other authors [42,43]. It is also noteworthy that the $[Ti(Cat)_3]^{2-}$ absorption band was only apparent at pH 6 and 9, which is in strong agreement with the results shown in Fig. 1a.

*3.2. Mechanism of Ti-catechol decomposition and coating formation*

Cyclic voltammetry (CV), a type of potentiodynamic electrochemical technique that provides insights into the redox reactions of compounds in solutions, was carried out to understand how “free” catechol and Ti-catechol complex decompose under conditions that roughly simulate those existing on the surface of arsenopyrite during oxidation. Cyclic voltammogram of catechol at pH 5 (Fig. 2a-1) showed an anodic peak at 770 mV vs. SHE ($A_1$) and a cathodic peak at 500 mV ($C_1$), which are consistent with the well-documented reversible redox reaction of this organic compound [29,47,48]. Catechol is oxidized to quinone (1,2-Benzoquinone) during the anodic sweep at 770 mV and is reduced back to catechol in the succeeding cathodic sweep at 500 mV (Eq. (2)). In contrast, the voltammogram of catechol at pH 9 (Fig. 2a-2) showed two anodic peaks at 260 ($A_1'$) and 780 mV ($A_2'$) but only one cathodic peak at 500 mV ($C_1'$). The peaks at $A_2'$ and $C_1'$ were similar to that of catechol at pH 5 while the additional anodic peak at

ca. 260 mV ($A_1'$) could be attributed to oxidation of semi-quinone (Eq. (3)) formed during solution preparation. The strong presence of semi-quinone at pH 9 could be explained by the following reasons: (1) faster oxidation rate of catechol to semi-quinone by $O_2$ under alkaline conditions [49], and (2) greater stability of semi-quinone because of its lower one-electron reduction potential at higher pH [48].

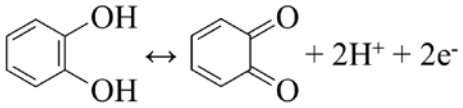


(2)

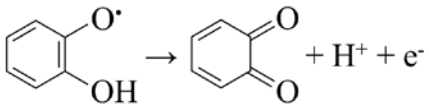


(3)

A new anodic peak at ca. 680 mV ($A_1''$) appeared in the cyclic voltammogram of Ti-catechol complex (Fig. 2a-3) indicating that the synthesized Ti-catechol complex, $[Ti(Cat)_3]^{2-}$, could undergo anodic decomposition. The cathodic peak observed at 440 mV ($C_1''$) was most likely due to the reduction of quinone to catechol as discussed earlier. In the second cycle (Fig. 2a-3), however, the anodic peak decreased and shifted towards higher potentials compared with that of the first cycle. Succeeding cycles (i.e., 3rd and 4th) also showed continuous shift and decrease of the anodic peak until it virtually disappeared on the fifth cycle. This gradual decrease of the anodic peak could be attributed to the decreasing amount of Ti-catechol complex due to its oxidative

decomposition near the surface of working electrode, which was not regenerated from oxidation products in the succeeding cathodic sweep. This means that the oxidative decomposition of Ti-catechol complex is irreversible. Furthermore, shifting of the anodic peak may suggest that the surface of platinum electrode is gradually being covered by oxidation products.

Some metal tris-catecholate complexes like those of Mn(IV) and Fe(III) have been reported to decompose sequentially [50], so to determine whether this is also the case for the synthesized Ti-catechol complex, CV measurements at several scan rates were conducted to vary the extent of oxidation-reduction reactions. Despite the use of various scan rates (1–30 mV/s), however, only one anodic peak was observed (Fig. 2b), indicating that the oxidative decomposition of Ti-catechol complex occurred via a one-step process and not sequentially. Satur et al. [21] proposed that the one-step oxidation of Ti-catechol complex occur via simultaneous oxidation of the three catechol molecules coordinated with $Ti^{4+}$, which would then be precipitated as Ti-hydroxide/oxide because of its very low solubility at pH > 4. If their hypothesis is correct, the product after oxidation would be composed almost entirely of Ti-hydroxide/oxide. To verify this, chronoamperometry was carried out at 1.0 V vs. SHE for 3 h to generate enough oxidation products on the Pt electrode for SEM-EDX

analysis. As illustrated in Fig. 3, there were two distinct materials observed in the coating formed on Pt electrode after chronoamperometry: (1) a high carbon-containing substance (Ti—O—C), and (2) a high titanium and oxygen-containing material (Ti—O). These materials are definitely oxidation products of Ti-catechol complex decomposition because they were not observed when the same experiment was done without applying any potential (Supplementary information, Fig. S2). Based on these results, decomposition of Ti-catechol is much more complicated than the earlier mechanism proposed by Satur et al. [21].

In the structure of Ti(IV) tris-catecholate complex (Fig. 4), one catechol molecule is "normally" coordinated with the central Ti4+ ion while the remaining two molecules are coordinated with distortions because of unpaired electrons in two oxygen atoms ($O_4$ and $O_5$) [42]. These oxygen atoms, $O_4$ and $O_5$, are relatively more reactive than the others, so during anodic decomposition, Ti-$O_4$ and/or Ti-$O_5$ bonds are most probably attacked first and dislodged, resulting in the formation of Ti(IV) mono- and/or bis-catecholate complex (Eqs. (4) and (5)). Mono- and bis-catecholate complexes have been reported for Mn(IV) and Fe(III) but not for Ti(IV), which could indicate that {Ti(Cat)} and/or {$Ti(Cat)_2$} complex(es) are very unstable individually [43,50]. However, they could react with each other and form more stable polymerized metal-organic molecules. In a

recent paper of Bazhenova et al. [51], a new family of polymerized Ti-catechol complexes were introduced that contain both $Ti^{4+}$ mono- and bis-catecholate complexes as their "elementary" components, suggesting that the presence of Ti—O—C "intermediate" was likely the result of partial oxidation-polymerization reactions.

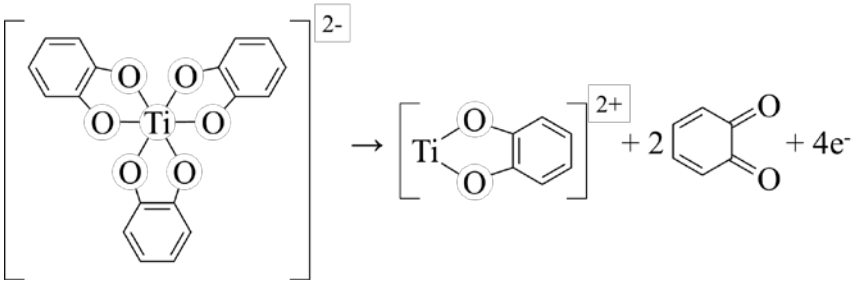


(4)

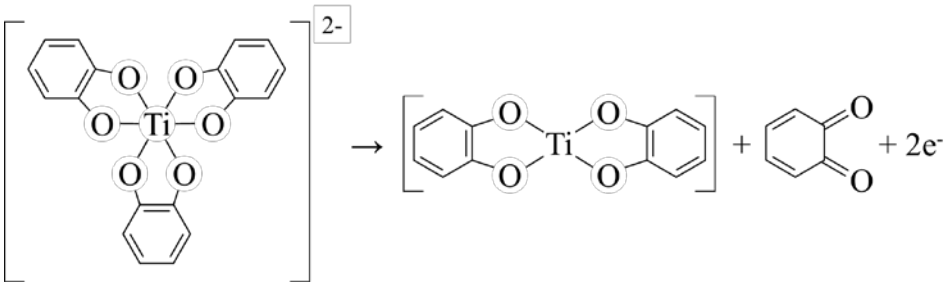


(5)

Ti—O in the coating, observed as regions with darker hues in the BSE image with very strong Ti and O signals (Fig. 3), was most likely formed by the decomposition of Ti—O—C "intermediate", which did not require electron transfer. This is consistent with the cyclic voltammogram of Ti-catechol complex showing a one-step electrochemical reaction (i.e., $[Ti(Cat)_3]^{2-}$ oxidation → Ti—O—C "intermediate" formation) (Fig. 2). Finally, $Ti^{4+}$ ion released from the intermediate was likely precipitated as Ti-hydroxide/oxide, which constitutes most of the Ti—O material in the Ti—O—C coating.

Based on these results, a three-step mechanism is proposed for the decomposition of Ti-catechol complex (Fig. 5). In Step 1, Ti-catechol complex is partially oxidized, most probably via the Ti-O distorted bonds, and forms an intermediate phase. After this, the intermediate is gradually dissociated until "free" $Ti^{4+}$ ion is released (Step 2). In the final step (Step 3), "free" $Ti^{4+}$ ion is hydrolyzed and precipitated to form Ti-oxyhydroxide coatings.

*3.3. Ti-based CME treatment of arsenopyrite*

The arsenopyrite sample used in this study was obtained from Toroku Mine, Miyazaki, Japan. XRD pattern of the sample shows that it is mainly composed of arsenopyrite with pyrite and quartz as minor minerals (Supplementary information, Fig. S3). Its chemical composition is 32.6, 30.9 and 20.1% of Fe, As and S, respectively, and these values translate to ca. 67% of arsenopyrite, 13% of pyrite and 15% of quartz (Supplementary information, Table S1).

Fig. 6 shows the evolution of pH, Eh, and concentrations of As and Ti in DI water (control), catechol only and Ti-catechol complex solution (CME). In the control, the pH rapidly decreased from 9 to 3.5 after 1 day due to the production of hydrogen ion by arsenopyrite oxidation [29,37], which is consistent with the redox potential (Eh) increase from ca. 250 to 500 mV (Fig. 6a and b). The oxidation of arsenopyrite with

time was also apparent in the rapid concentration increase of As in the control that reached ca. 1000 mg/L after 7 days (Eqs. (6)–(8)). After this period, the change in As concentration with time became statistically insignificant indicating that apparent equilibrium was reached.

$$4FeAsS_{(s)} + 11O_{2(aq)} + 6H_2O \rightarrow 4Fe^{2+}_{(aq)} + 4H_3AsO_{3(aq)} + 4SO_4^{2-}{}_{(aq)} \quad (6)$$

$$4Fe^{2+}_{(aq)} + O_{2(aq)} + 4H^{+}_{(aq)} \rightarrow 4Fe^{3+}_{(aq)} + 2H_2O \quad (7)$$

$$FeAsS_{(s)} + 13Fe^{3+}_{(aq)} + 8H_2O \rightarrow 14Fe^{2+}_{(aq)} + H_3AsO_{4(aq)} + SO_4^{2-}{}_{(aq)} + 13H^{+}_{(aq)} \quad (8)$$

In the presence of catechol, As concentration was lower and the pH was higher compared with those of the control (Fig. 6a and c), which means that arsenopyrite oxidation was somehow limited by this organic compound. This suppressive effect could be explained by two possible mechanisms. First, catechol adsorption to the surface of arsenopyrite may suppress the overall dynamics of arsenopyrite oxidation by protecting the mineral from oxidants. This “direct” effect of catechol is most likely similar to that previously reported by Lalvani et al. [52] and Belzile et al. [53] on pyrite passivation by humic acids, large organic molecules that contain catechol as one of their most common functional groups. Noteworthy in the results was the continuous increase of As concentration with time in the catechol only solution, which suggests that although arsenopyrite oxidation was minimized, the mineral was not passivated by

catechol (Fig. 6c). Second, catechol could “indirectly” suppress arsenopyrite oxidation by consuming DO and complexing with $Fe^{3+}$, both of which are essential oxidants of arsenopyrite. According to Pracht et al. [28], catechol consumes DO and metal ions such as $Fe^{3+}$ in its oxidation to quinone (Eqs. (9) and (10)). Ferric ion has also been reported to form several stable complexes with catechol (e.g., Eq. (11)) preventing it from directly acting as an oxidant of arsenopyrite [29]. The combined effects of adsorption, consumption of oxidants and formation of Fe(III)-catechol complexes could explain the decrease in As concentration observed in the presence of catechol.

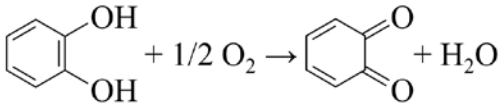


(9)

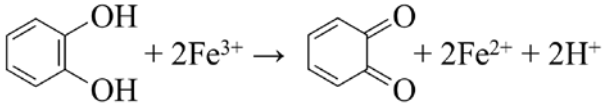


(10)

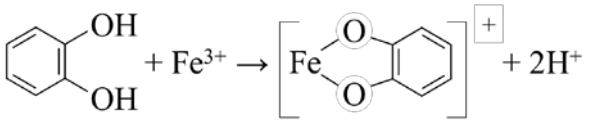


(11)

The amounts of As released from arsenopyrite was even lower in Ti-catechol complex solution (CME) compared with the other two cases (Fig. 6c). After 25 days, As concentration in CME was ca. 330 mg/L, which was roughly four-fold lower than the control (1150 mg/L) and less than half of that in catechol only solution (880 mg/L). The

pH was also higher in CME compared with the other cases while Eh was the lowest (Fig. 6a and b). These results suggest that the substantial decrease in As release from arsenopyrite could be attributed to passivation of the mineral itself by Ti-catechol complex. The passivation of arsenopyrite was closely related to $Ti^{4+}$ precipitation that was apparent in the concentration decrease of dissolved Ti with time, which was not observed in Ti-catechol solution without arsenopyrite (Fig. 6d). SEM-EDX results also showed that arsenopyrite in CME after 25 days exhibited strong signals of Ti and O (Fig. 7). Coating coverage was estimated at roughly 60 % using image analysis of Ti elemental maps from SEM-EDX (Supplementary information, Fig. S4 and Table S2). The nature of this passivation layer was characterized using DRIFTS, a surface-sensitive technique able to identify molecular coordinations of ions and molecules in the structure of minerals [54] including the very thin oxidation products of pyrite oxidation [19,26,55]. The DRIFTS spectra of washed arsenopyrite and leached residues (control, catechol and CME) show that several oxidation products were formed on arsenopyrite (Fig. 8a). Absorption bands at 457 and 792 $cm^{-1}$ are assigned to vibrations of Fe-As and arsenate (O-As-O), respectively. The stronger signal of arsenate (792 $cm^{-1}$) in the control indicates that arsenopyrite oxidation was more extensive in DI water compared with those in the other cases [56,57]. Absorption bands at 569, 487 and

478 $cm^{-1}$ are assigned to Fe-O bonds of iron oxide and the peak at 1371 $cm^{-1}$ is most likely due to $Fe^{3+}$-OH band of $Fe^{3+}$-hydroxides or oxyhydroxides [26,57,58]. Vibrations of sulfate coordinated with $Fe^{3+}$ and $Fe^{2+}$ were also observed at 1050 and 1163 $cm^{-1}$, respectively [54–58]. The wide peak between 1115 and 1230 $cm^{-1}$ is assigned to the vibrations of C-H (1165 $cm^{-1}$), O-H (1187 $cm^{-1}$), and C-O (1193 $cm^{-1}$), indicating two possibilities: (1) adsorbed catechol on arsenopyrite [59], and (2) an "intermediate" phase formed on arsenopyrite by the partial decomposition of Ti-catechol complex as discussed previously. The deconvoluted spectrum between 500 and 400 $cm^{-1}$ of arsenopyrite leached in Ti-catechol complex solution (Fig. 8b) shows several absorption bands at 488, 474, 445 and 427 $cm^{-1}$, which are consistent with Ti-O vibrations of anatase (β-$TiO_2$) [60–63]. This means that the Ti and O signals detected by SEM-EDX were likely due to the Ti-oxide coating formed on arsenopyrite that passivated the mineral itself and limited the release of As.

## 4. Conclusion

This study investigated the formation of Ti-catechol complex, its electrochemical properties and its application to the CME treatment of arsenopyrite. The findings of this study are summarized as follows:

1) Ti-catechol complex was successfully synthesized by rapid neutralization of very acidic $Ti^{4+}$ and catechol solutions to pH > 5.

2) The synthesized Ti-catechol complex had a tris-catecholate configuration, $[Ti(Cat)_3]^{2-}$, and was relatively stable between pH 5 and 12.

3) $[Ti(Cat)_3]^{2-}$ could be oxidized at 680 mV most probably via partial oxidation of either one or both of the catechol molecules with distorted Ti-O bonds. The partially oxidized complex(es) likely reacted with each other to form an “intermediate” phase composed of Ti, O and C.

4) Under certain conditions, the “intermediate” could be completely dissociated, which released “free” $Ti^{4+}$ ion into solution that rapidly precipitated as $TiO_2$.

5) Ti-based CME suppressed the release of As from arsenopyrite by coating the mineral with Ti-oxide.

6) The new method to synthesize Ti-catechol complex and the added insights into the mechanisms of CME treatment could help in the design of practical approaches to mitigate not only the release of As but also the formation of AMD.

## Acknowledgments

A part of this study was financially supported by the Japan Society for the Promotion

of Science (JSPS) grant-in-aid for scientific research (Grant numbers: 26820390, 17H03503 and 17K12831). We also wish to thank Dr. Gianluca Li Puma and the anonymous reviewers for their valuable inputs to this paper.

## References

[1] D. Banks, P.L. Younger, R.T. Arnesen, E.R. Iversen, S.B. Banks, Mine-water chemistry: the good, the bad and the ugly, Environ. Geol. 32 (1997) 157–174.

[2] A.R. Elsetinow, M.J. Borda, M.A.A. Schoonen, D.R. Strongin, Suppression of pyrite oxidation in acidic aqueous environments using lipids having two hydrophobic tails, Adv. Environ. Res. 7 (2003) 969–974.

[3] D.B. Johnson, K.B. Hallberg, Acid mine drainage remediation options: a review, Sci. Total Environ. 338 (2005) 3–14.

[4] C.B. Tabelin, T. Igarashi, Mechanisms of arsenic and lead release from hydrothermally altered rock, J. Hazard. Mater. 169 (2009) 980–990.

[5] C.B. Tabelin, T. Igarashi, R. Takahashi, The roles of pyrite and calcite in the mobilization of arsenic and lead from hydrothermally altered rocks excavated in Hokkaido, Japan, J. Geochem. Explor. 119 (2012) 17–31.

[6] C.B. Tabelin, A.H.M. Basri, T. Igarashi, T. Yoneda, Removal of arsenic, boron, and selenium from excavated rocks by consecutive washing, Water Air Soil Poll. 223 (2012) 4153–4167.

[7] C.B. Tabelin, T. Igarashi, T. Arima, D. Sato, T. Tatsuhara, S. Tamoto, Characterization and evaluation of arsenic and boron adsorption onto natural geologic materials, and their application in the disposal of excavated altered rock, Geoderma 213 (2012) 163–172.

[8] C.B. Tabelin, T. Igarashi, R. Takahashi, Mobilization and speciation of arsenic from hydrothermally altered rock in laboratory column experiments under ambient conditions, Appl. Geochem. 27 (2012) 326–342.

[9] C.B. Tabelin, A. Hashimoto, T. Igarashi, T. Yoneda, Leaching of boron, arsenic and selenium from sedimentary rocks: I. Effects of contact time, mixing speed and liquid-to-solid ratio,

Sci. Total Environ. 472 (2014) 620–629.

[10] C.B. Tabelin, A. Hashimoto, T. Igarashi, T. Yoneda, Leaching of boron, arsenic and selenium from sedimentary rocks: II. pH dependence, speciation and mechanisms of release, Sci. Total Environ. 473–474 (2014) 244–253.

[11] C.B. Tabelin, R. Sasaki, T. Igarashi, I. Park, S. Tamoto, T. Arima, M. Ito, N.Hiroyoshi, Simultaneous leaching of arsenite, arsenate, selenite and selenite, and their migration in tunnel-excavated sedimentary rocks: I. Column experiments under intermittent and unsaturated flow, Chemosphere 186(2017) 558–569.

[12] C.B. Tabelin, R. Sasaki, T. Igarashi, I. Park, S. Tamoto, T. Arima, M. Ito, N.Hiroyoshi, Simultaneous leaching of arsenite, arsenate, selenite and selenite, and their migration in tunnel-excavated sedimentary rocks: II. Kinetic and reactive transport modeling, Chemosphere (2017), http://dx.doi.org/10.1016/j.chemosphere.2017.08.088 (Accepted).

[13] T. Tatsuhara, T. Arima, T. Iagarashi, C.B. Tabelin, Combinedneutralization-adsorption system for the disposal of hydrothermally altered excavated rock producing acidic leachate with hazardous elements, Eng. Geol.139–140 (2012) 76–84.

[14] S. Tamoto, C.B. Tabelin, T. Igarashi, M. Ito, N. Hiroyoshi, Short and long term release mechanisms of arsenic selenium and boron from tunnel-excavated sedimentary rock under in situ conditions, J. Contam. Hydrol. 175–176 (2015)60–71.

[15] A. Akcil, S. Koldas, Acid Mine Drainage (AMD): causes, treatment and case studies, J. Clean. Prod. 14 (2006) 1139–1145.

[16] B. Gazea, K. Adam, A. Kontopoulos, A review of passive systems for the treatment of acid mine drainage, Miner. Eng. 9 (1996) 23–42.

[17] N.F. Gray, Environmental impact and remediation of acid mine drainage: a management problem, Environ. Geol. 30 (1997) 62–71.

[18] A.N. Shabalala, S.O. Ekolu, S. Diop, F. Solomon, Pervious concrete reactive barrier for removal of heavy metals from acid mine drainage-column study, J. Hazard. Mater. 323 (2017) 641–653.

[19] V.P. Evangelou, Pyrite Oxidation and Its Control, CRC press, Boca Raton, FL, 1995.

[20] V.P. Evangelou, Pyrite microencapsulation technologies: principles and potential field application, Ecol. Eng. 17 (2001) 165–178.

[21] J. Satur, N. Hiroyoshi, M. Tsunekawa, M. Ito, H. Okamoto, Carrier-microencapsulation for

preventing pyrite oxidation, Int. J. Miner. Eng.83 (2007) 116–124.

[22] R.K.T. Jha, J. Satur, N. Hiroyoshi, M. Ito, M. Tsunekawa, Carrier-microencapsulation using Si-catechol complex for suppressing pyrite floatability, Miner. Eng. 21 (2008) 889–893.

[23] R.K.T. Jha, J. Satur, N. Hiroyoshi, M. Ito, M. Tsunekawa, Suppression of floatability of pyrite in coal processing by carrier microencapsulation, Fuel Process. Technol. 92 (2011) 1032–1036.

[24] M.D. Yuniati, K. Kitagawa, T. Hirajima, H. Miki, N. Okibe, K. Sasaki, Suppression of pyrite oxidation in acid mine drainage by carrier microencapsulation using liquid product of hydrothermal treatment of low-rank coal, and electrochemical behavior of resultant encapsulating coatings, Hydrometallurgy 158 (2015) 83–93.

[25] J.D. Rimstidt, D.J. Vaughan, Pyrite oxidation: a state-of-the-art assessment of the reaction mechanism, Geochim. Cosmochim. Acta 67 (2003) 873–880.

[26] C.B. Tabelin, S. Veerawattananun, M. Ito, N. Hiroyoshi, T. Igarashi, Pyrite oxidation in the presence of hematite and alumina: I. Batch leaching experiments and kinetic modeling calculations, Sci. Total Environ. 580 (2017)687–698.

[27] C.B. Tabelin, S. Veerawattananun, M. Ito, N. Hiroyoshi, T. Igarashi, Pyrite oxidation in the presence of hematite and alumina: II. Effects on the cathodic and anodic half-cell reactions, Sci. Total Environ. 581–582 (2017) 126–135.

[28] J. Pracht, J. Boenigk, M. Isenbeck-Schröter, F. Keppler, H.F. Schöler, Abiotic Fe(III) induced mineralization of phenolic substances, Chemosphere 44 (2001) 613–619.

[29] N. Schweigert, A.J.B. Zehnder, R.I.L. Eggen, Chemical properties of catechols and their molecular modes of toxic action in cells, from microorganisms to mammals, Environ. Microbiol. 3 (2001) 81–91.

[30] C.L. Corkhill, D.J. Vaughan, Arsenopyrite oxidation − a review, Appl. Geochem.24 (2009) 2342–2361.

[31] S. Coussy, M. Benzaazoua, D. Blanc, P. Moszkowicz, B. Bussière, Arsenic stability in arsenopyrite-rich cemented paste backfills: a leaching test-based assessment, J. Hazard. Mater. 185 (2011) 1467–1476.

[32] A.B.M.R. Islam, J.P. Maity, J. Bundschuh, C.Y. Chen, B.K. Bhowmik, K. Tazaki, Arsenic mineral dissolution and possible mobilization in mineral-microbe-groundwater environment, J. Hazard. Mater. 262 (2013) 989–996.

[33] A. Murciego, E. Álvarez-Ayuso, E. Pellitero, M.A. Rodríguez, A. García-Sánchez, J. Tamayo, J. Rubio, F. Rubio, J. Rubin, Study of arsenopyrite weathering products in mine wastes from abandoned tungsten and tin exploitations, J. Hazard. Mater. 186 (2011) 590–601.

[34] K.A. Salzsauler, N.V. Sidenko, B.L. Sherriff, Arsenic mobility in alteration products of sulfide-rich arsenopyrite-bearing mine wastes, Snow Lake, Manitoba, Canada, Appl. Geochem. 20 (2005) 2303–2314.

[35] A. Basu, M.E. Schreiber, Arsenic release from arsenopyrite weathering: insights from sequential extraction and microscopic studies, J. Hazard. Mater.262 (2013) 896–904.

[36] C.K. Jain, I. Ali, Arsenic: occurrence, toxicity and speciation techniques, Water Res. 34 (2000) 4304–4312.

[37] D. Mohan, C.U. Pittman Jr., Arsenic removal from water/wastewater using adsorbents − a critical review, J. Hazard. Mater. 142 (2007) 1–53.

[38] H.W. Nesbitt, I.J. Muir, A.R. Pratt, Oxidation of arsenopyrite by air and air-saturated distilled water, and implications for mechanism of oxidation, Geochim. Cosmochim. Acta 59 (1995) 1773–1786.

[39] S. Agatzini-Leonardou, P. Oustadakis, P.E. Tsakiridis, Ch. Markopoulos, Titanium leaching from red mud by diluted sulfuric acid at atmospheric pressure, J. Hazard. Mater. 157 (2008) 579–586.

[40] S. He, H. Sun, D. Tan, T. Peng, Recovery of titanium compounds from Ti-enriched product of alkali melting Ti-bearing blast furnace slag by dilute sulfuric acid leaching, Procedia Environ. Sci. 31 (2016) 977–984.

[41] F.C. Meng, T.Y. Xue, Y.H. Liu, G.Z. Zhang, T. Qi, Recovery of titanium from undissolved residue (tionite) in titanium oxide industry via NaOH hydrothermal conversion and $H_2SO_4$ leaching, Trans. Nonferrous Met. Soc. China 26 (2016) 1696–1705.

[42] B.A. Borgias, S.R. Cooper, Y.B. Koh, K.N. Raymond, Synthetic structural, and physical studies of titanium complexes of catechol and 3,5-Di-tert-butylcatechol, Inorg. Chem. 23 (1984) 1009–1016.

[43] M.J. Sever, J.J. Wilker, Visible absorption spectra of metal-catecholate and metal-tironate complexes, Dalton Trans. (2004) 1061–1072.

[44] M.A. McKibben, B.A. Tallant, J.K. del Angel, Kinetics of inorganic arsenopyrite oxidation

in acidic aqueous solutions, Appl. Geochem. 23 (2008) 121–135.

[45] C.M. Bethke, The Geochemist's Workbench −A User's Guide to Rxn, Act2, Tact, React and Gtplot, University of Illinois, Urbana Illinois, 1992.

[46] J.P. Gustafsson, Visual MINTEQ Thermodynamic Databases in GWB Format, 2010, http://vminteq.lwr.kth.se. (Accessed 08 April 2010).

[47] J.C. Danilewicz, Review of oxidative processes in wine and value of reduction potentials in enology, Am. J. Enol. Vitic. 63 (2012) 1–10.

[48] J. Yang, M.A.C. Stuart, M. Kamperman, Jack of all trades: versatile catechol crosslinking mechanisms, Chem. Soc. Rev. 43 (2014) 8271–8298.

[49] C.I. Wright, H.S. Mason, The oxidation of catechol by tyrosinase, J. Biol. Chem.165 (1946) 45–53.

[50] K.A. Boles, Electrochemistry of tris(tetrachlorocatecholate) complexes of manganese, iron, and cobalt, Chem. Biochem. Graduate Theses Dissertations (2014).

[51] T.A. Bazhenova, N.V. Kovaleva, G.V. Shilov, G.N. Petrova, D.A. Kuznetsov, A family of titanium complexes with catechol ligands: structural investigation and catalytic application, Eur. J. Inorg. Chem. 33 (2016) 5215–5221.

[52] S.B. Lalvani, B.A. Deneve, A. Weston, Passivation of pyrite due to surface treatment, Fuel 69 (1990) 1567–1569.

[53] N. Belzile, S. Maki, Y.W. Chen, D. Goldsack, Inhibition of pyrite oxidation by surface treatment, Sci. Total Environ. 196 (1997) 177–186.

[54] L. Carlson, J.M. Bingham, U. Schwertmann, A. Kyek, F. Wagner, Scavenging of As from acid mine drainage by schwertmannite and ferrihydrite: a comparison with synthetic analogues, Environ. Sci. Technol. 36 (2002) 1712–1719.

[55] M.J. Borda, D.R. Strongin, M.A. Schoonen, A vibrational spectroscopic study of the oxidation of pyrite by molecular oxygen, Geochim. Cosmochim. Acta 68 (2004) 1807–1813.

[56] M. Achimovi˘cová, P. Balá˘z, Influence of mechanical activation on selectivity of acid leaching of arsenopyrite, Hydrometallurgy 77 (2005) 3–7.

[57] M.B.M. Monte, A.J.B. Dutra, C.R.F. Albuquerque Jr., L.A. Tondo, F.F. Lins, The influence of the oxidation state of pyrite and arsenopyrite on the flotation of an auriferous sulphide ore, Miner. Eng. 15 (2002) 1113–1120.

[58] I.V. Chernyshova, An in situ FTIR study of galena and pyrite oxidation in aqueous solution,

J. Electroanal. Chem. 558 (2003) 83–98.

[59] F.J. Ramírez, J.T. López Navarrete, Normal coordinate and rotational barrier calculations on 1,2-dihydroxybenzene, Vib. Spectrosc. 4 (1993) 321–334.

[60] M.J. Alam, D.C. Cameron, Preparation and characterization of $TiO_2$ thin films by sol-gel method, J. Sol-Gel Sci. Technol. 25 (2002) 137–145.

[61] S. Bagheri, K. Shameli, S.B.A. Hamid, Synthesis and characterization of anatase titanium dioxide nanoparticles using egg white solution via sol-gel method, J. Chem. (2013) 1–5.

[62] Y. Djaoued, S. Badilescu, P.V. Ashrit, D. Bersani, P.P. Lottici, R. Brüning, Lowtemperature sol-gel preparation of nanocrystalline $TiO_2$ thin films, J. Sol-GelSci. Technol. 24 (2002) 247–254.

[63] Y. Djaoued, S. Badilescu, P.V. Ashrit, D. Bersani, P.P. Lottici, J. Robichaud, Study of anatase to rutile phase transition in nanocrystalline titania films, J. Sol-Gel Sci. Technol. 24 (2002) 255–264.

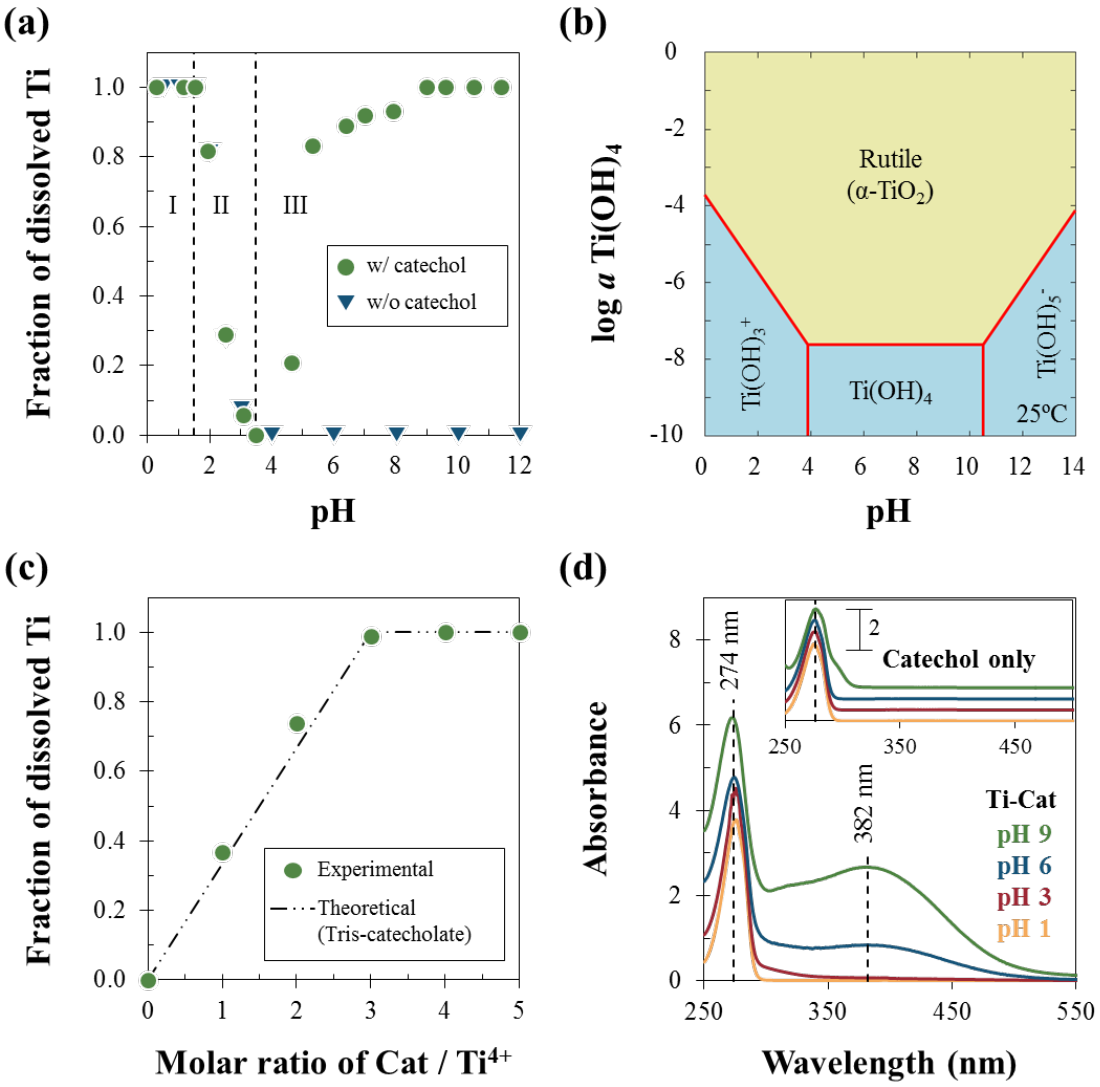


**Fig. 1.** Properties of synthesized Ti-catechol complex: (a) $Ti^{4+}$ ion stability with pH in the presence and absence of catechol, (b) Log a − pH predominance diagram of $Ti(OH)_4$ at 25ºC and 1.013 bar created using the Geochemist's Workbench® with MINTEQ database [45] and [46], (c) $Ti^{4+}$ion stability as a function of molar ratio of catechol to $Ti^{4+}$,(d) UV–vis spectra of "free" catechol and Ti-catechol solutions at pH 1, 3, 6 and 9.

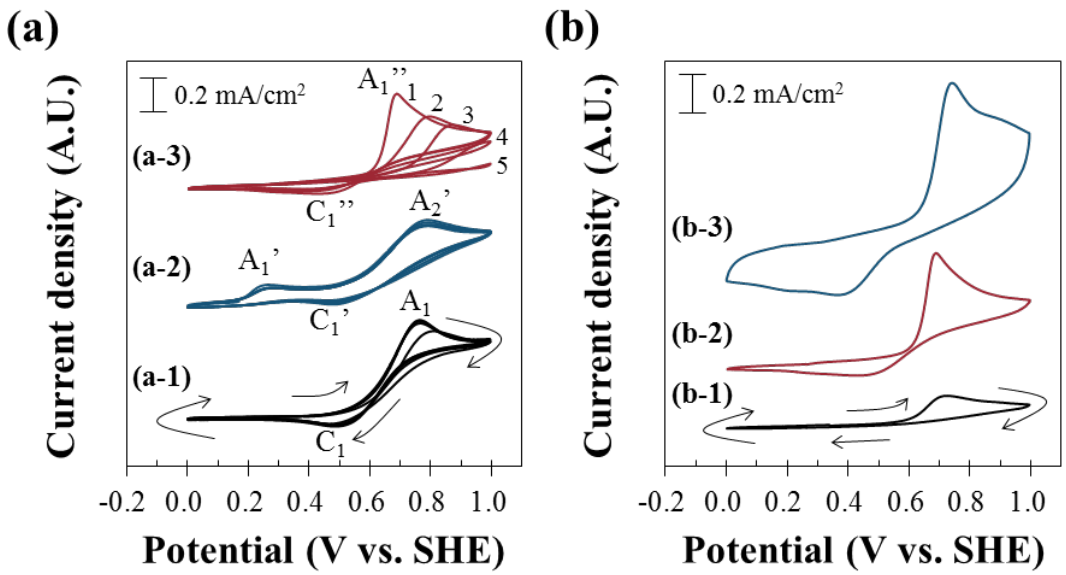


**Fig. 2.** Cyclic voltammograms of (a) catechol only and Ti-catechol solution at a scan rate of 5 mV/s, (a-1) catechol at pH 5, (a-2) catechol at pH 9, (a-3) Ti-catechol at pH 9, and (b) Ti-catechol solution at pH 9 with various scan rates (1 mV/s (b-1), 5 mV/s (b-2), and 30 mV/s (b-3)). Note that arrows denote the sweep direction.

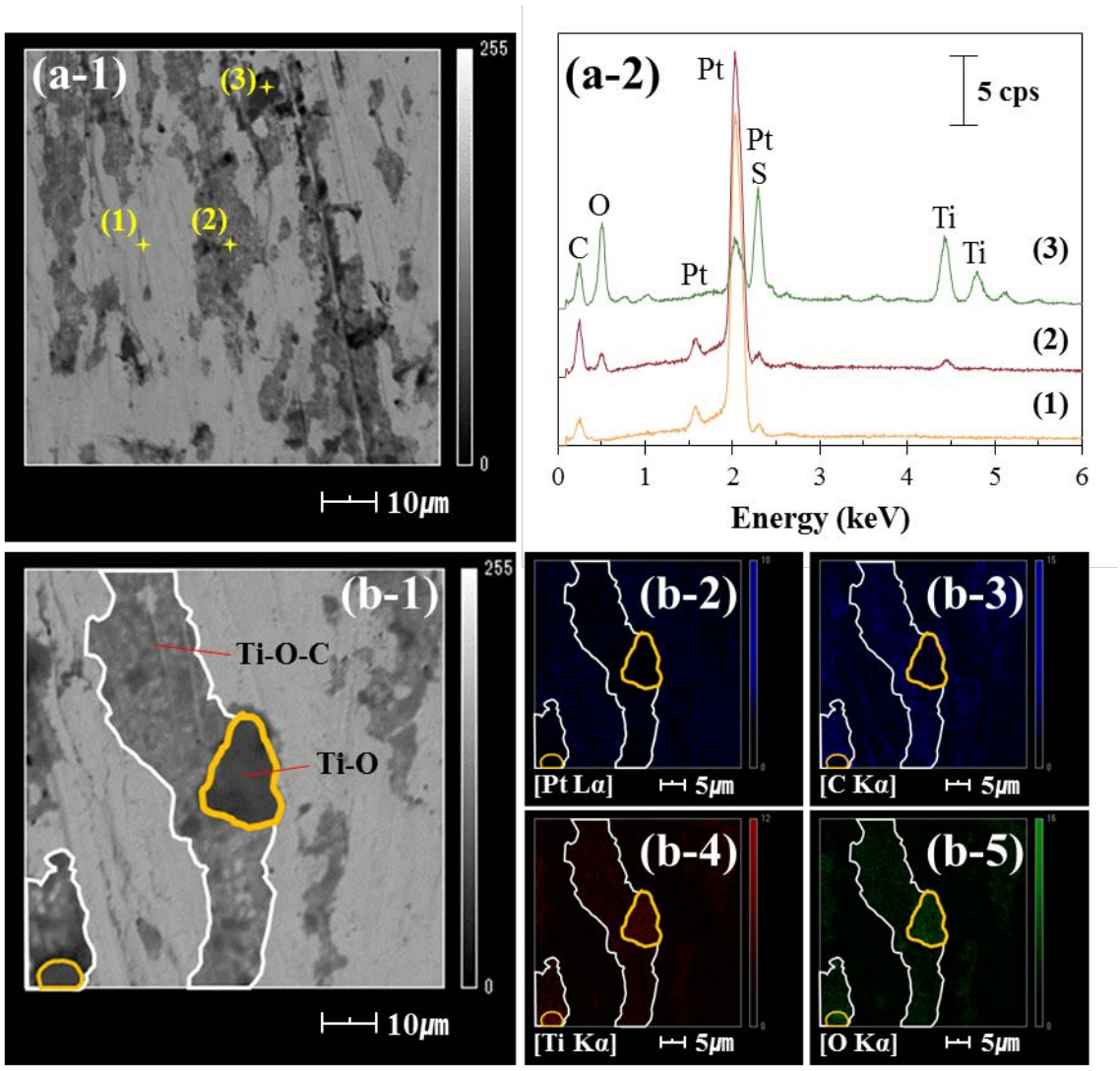


**Fig. 3.** SEM-EDX analysis of Pt electrode after chronoamperometry at 1.0 V vs. SHE for 3 h: (a-1) SEM photomicrograph and (a-2) energy dispersive X-ray spectra of several points, (b-1) SEM photomicrograph and the corresponding elemental maps of Pt (b-2), C (b-3), Ti (b-4), and O (b-5).

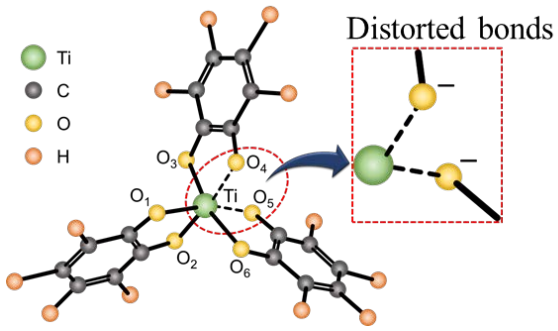


**Fig. 4.** Molecular structure of Ti(IV) tris-catecholate complex [42].

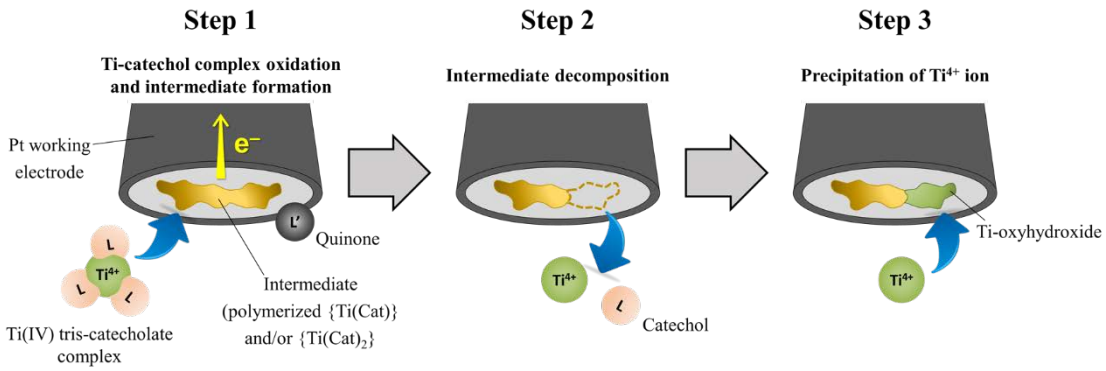


**Fig. 5.** A schematic diagram of the anodic decomposition of Ti-catechol complex.

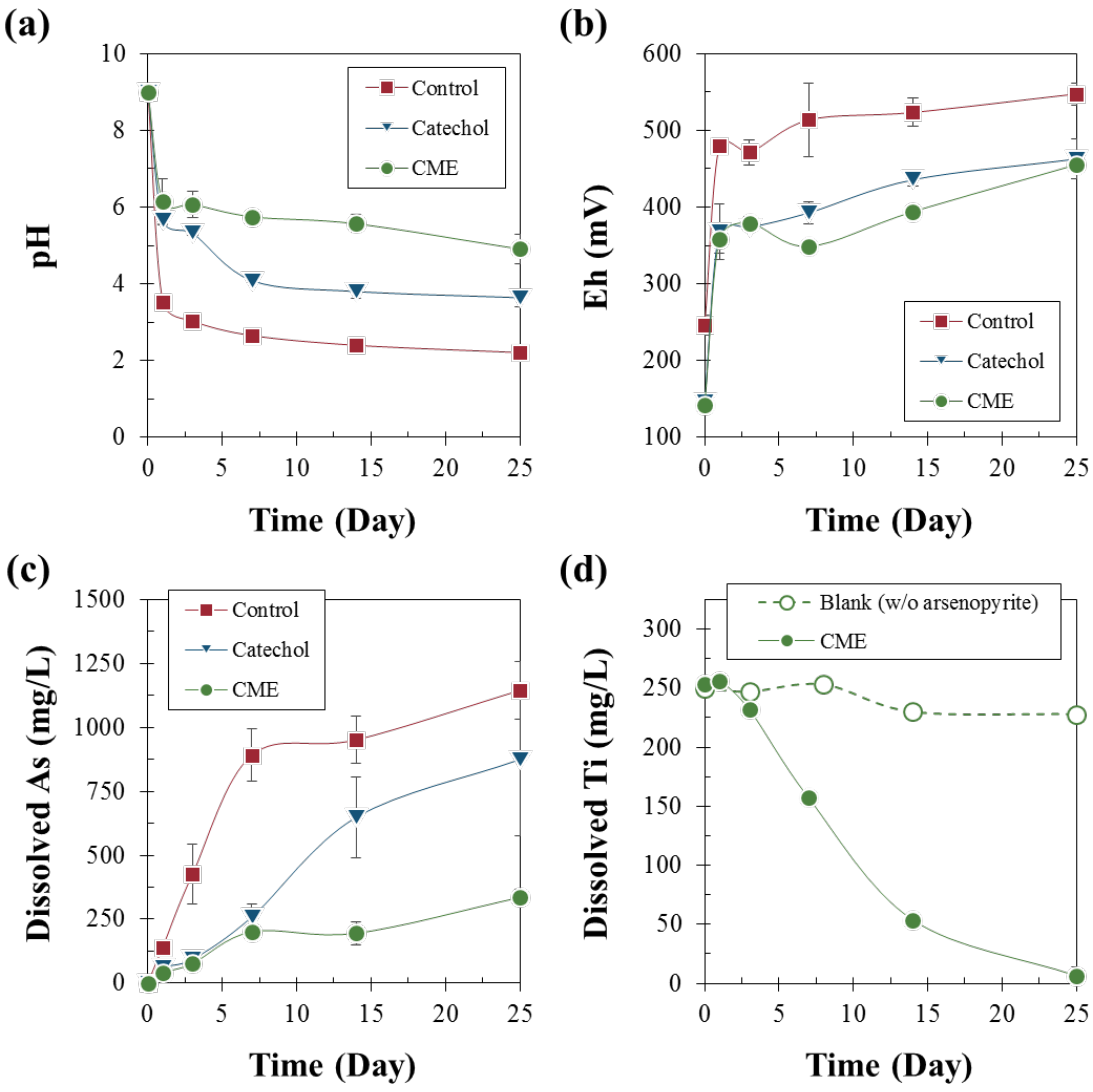


**Fig. 6.** Leaching of arsenopyrite in DI water (control), catechol only and Ti-catechol complex (CME): evolution of (a) pH and (b) Eh, and changes in the concentrations of (c) As and (d) Ti with time.

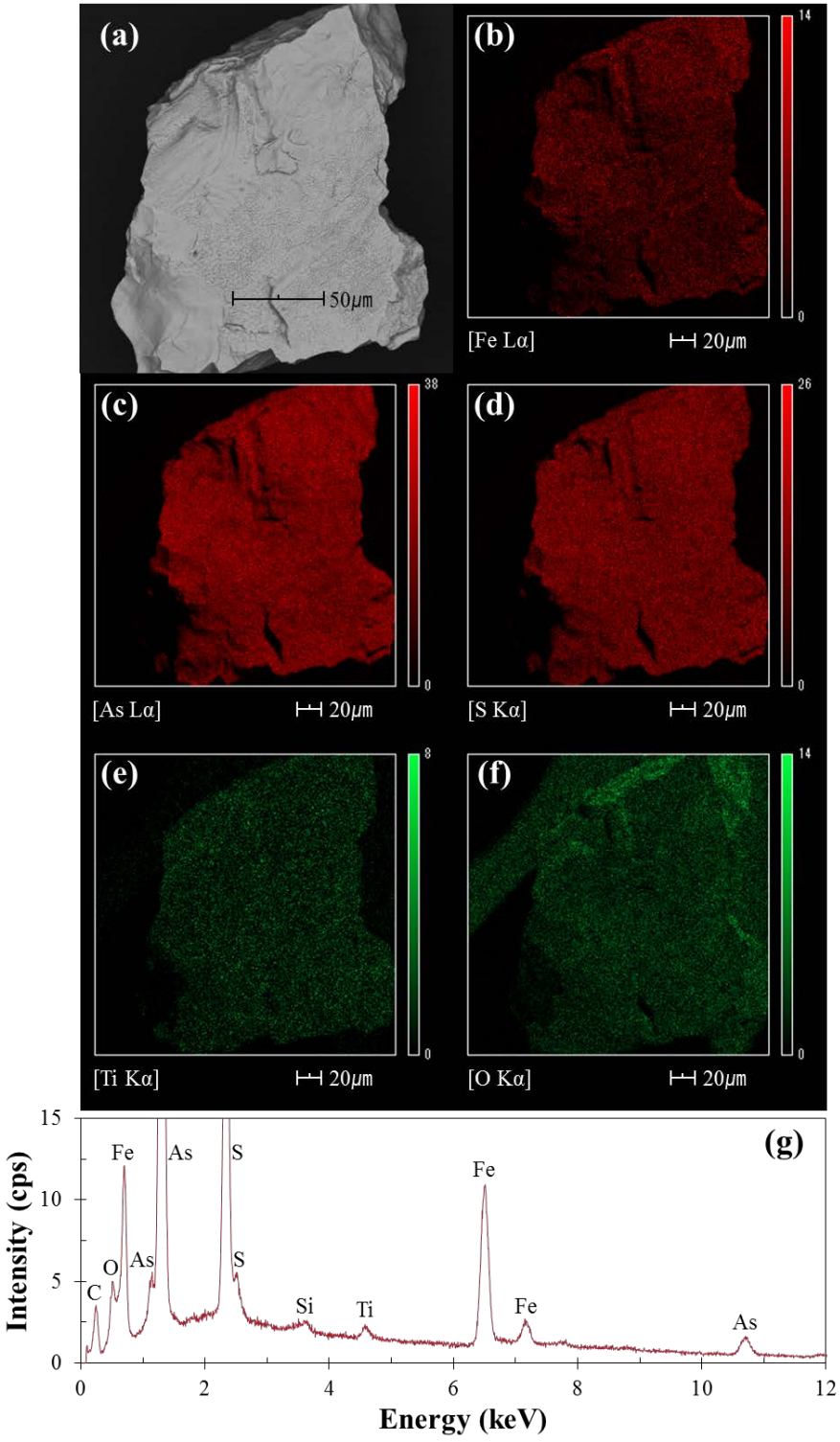


**Fig. 7.** SEM-EDX analysis of arsenopyrite after Ti-based CME treatment: (a) SEM photomicrograph, elemental maps of (b) Fe, (c) As, (d) S, (e) Ti and (f) O, and (g) energy dispersive X-ray spectrum of scanned area.

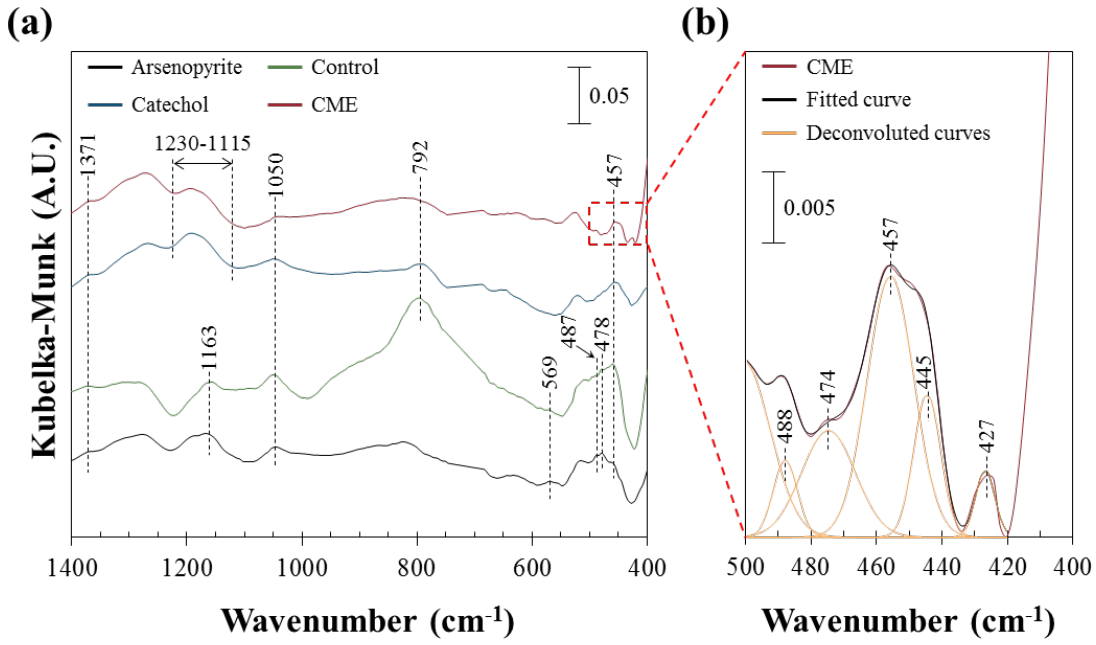


**Fig. 8.** DRIFTS spectra of arsenopyrite before and after 25 days of leaching experiments: (a) spectra of washed arsenopyrite and residues leached in DI water (control), catechol only and Ti-catechol solution (CME), and (b) deconvoluted spectrum of CME-treated arsenopyrite. Note that the scale of (a) and (b) are 0.05 and 0.005, respectively.

# Suppression of the release of arsenic from arsenopyrite by carrier-microencapsulation using Ti-catechol complex

Ilhwan Park, Carlito Baltazar Tabelin, Kagehiro Magaribuchi, Kensuke Seno, Mayumi Ito, Naoki Hiroyoshi

## Supplementary information

### Electrochemical studies

Cyclic voltammetry and chronoamperometry were performed using SI 128B electrochemical measurement unit (Solartron Instruments, UK) with a conventional three-electrode system (Fig. S1). Platinum (Pt) electrode, platinum wire and Ag/AgCl electrode filled with 3.3 M NaCl were used as working, counter and reference electrodes, respectively. Prior to the measurements, the solutions were filtered through 0.2 μm syringe-driven membrane filters. The filtered solution was poured into a glass reactor with water jacket, and equilibrated to 25°C for 40 minutes by recirculating water connected to a low-temperature water bath (BB400, Yamamoto Scientific Co. Ltd., Japan). After this, ultrapure $N_2$ (99.99 %) gas was introduced into the solution for 20 minutes to remove dissolved $O_2$ (DO).

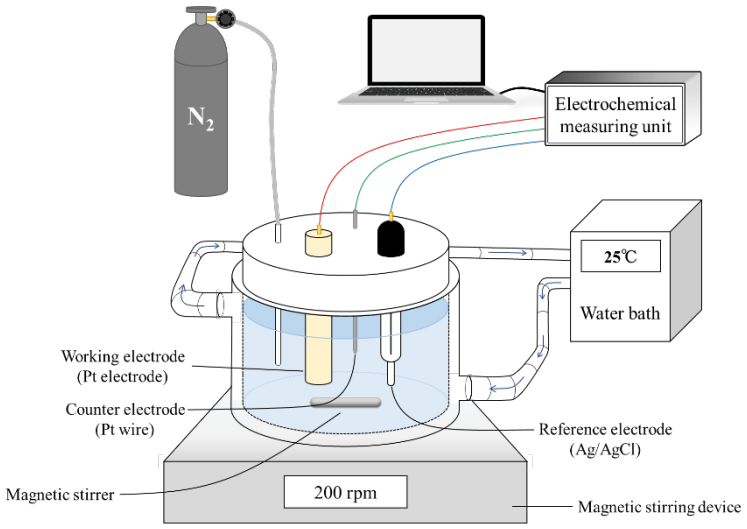


**Fig. S1.** A schematic diagram of the setup for electrochemical studies.

**The adsorption of Ti-catechol complex on Pt electrode**

After chronoamperometry at 1.0 V vs. SHE for 3 h, two types of coatings were formed on the Pt electrode: (1) Ti-O-C, and (2) Ti-O coating. These coatings might be formed by not only oxidation but also adsorption of Ti-catechol complex. To confirm whether adsorption of Ti-catechol was substantial, the same experiment was carried out but without applying potential. After that, Pt electrode was washed with deionized (DI) water and analyzed by SEM-EDX. As shown in Fig. S2 (a), the products, observed after chronoamperometry, were not formed on the surface of Pt electrode, and EDX spectra of several points (Fig. S2 (b)) showed only Pt and C signals, indicating that Ti-O-C and Ti-O coatings were most likely formed because of oxidation of Ti-catechol complex.

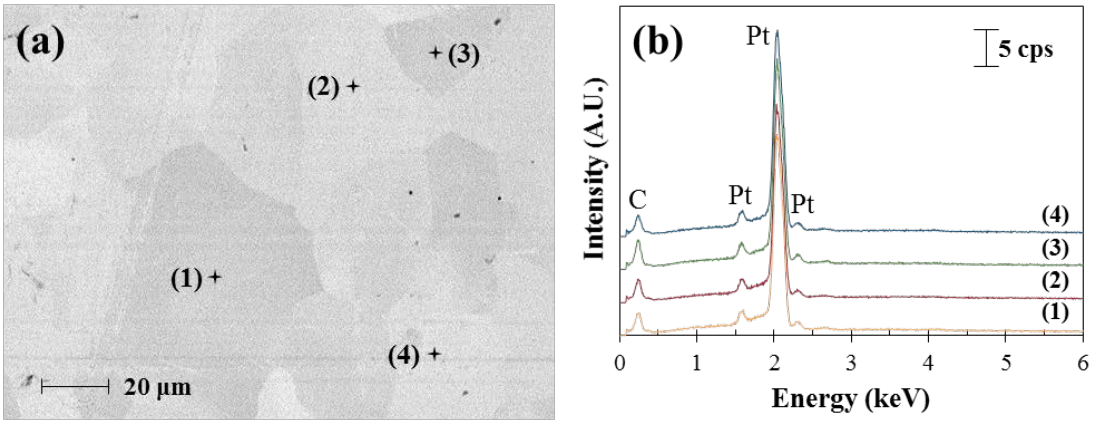


**Fig. S2.** SEM-EDX analysis of Pt electrode after immersion in Ti-catechol solution for 3 h: (a) SEM photomicrograph and (b) energy dispersive X-ray spectra of several points.

**Characterization of the arsenopyrite sample**

The arsenopyrite sample used in this study was obtained from Toroku Mine, Miyazaki, Japan. It was crushed by a jaw crusher (BB 51, Retsch Inc., Germany), ground by a disk mill (RS 100, Retsch Inc., Germany) and screened to obtain a size fraction of 106-150 μm in diameter. For its mineralogical characterization, the sample was further ground to <50 μm and analyzed by X-ray powder diffraction (XRD, MultiFlex, Rigaku Corporation, Japan) under the following conditions: radiation, Cu Kα, 40 kV, 40 mA; scan speed, 2 deg/min; angle range, 20-70°/2$\theta$. The XRD pattern of arsenopyrite sample shows that it is mainly composed of arsenopyrite with pyrite and quartz as minor minerals (Fig. S3).

The chemical composition of the sample was determined by wet method, which involves the dissolution of 100 mg of sample with 5 ml of 12 M HCl and 3 ml of 16 M $HNO_3$ (Wako Chemical Co. Ltd., Japan) using microwave-assisted acid digestion (Ethos, Milestone Inc., USA) and analyses of the leachate by inductively coupled plasma atomic emission spectrometer (ICP-AES, ICPE-9820, Shimadzu Corporation, Japan) (margin of error = ± 2%). The chemical composition of the sample is 32.6, 30.9 and 20.1% of Fe, As and S, respectively, and these values are equivalent to ca. 67% of arsenopyrite, 13% of pyrite and 15% of quartz (Table S1).

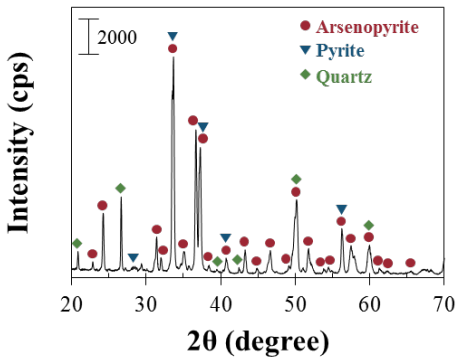


**Fig. S3.** Mineralogical composition of the arsenopyrite sample.

**Table S1.** Chemical composition of the arsenopyrite sample.

| **Elements** | Fe | As | S | Na | Mg | Cu | Al | Others |
|---|---|---|---|---|---|---|---|---|
| **wt. %** | 32.6 | 30.9 | 20.1 | 0.5 | 0.4 | 0.3 | 0.1 | 15.1 |

**Estimation of the coating coverage**

To estimate the coating coverage on arsenopyrite after CME treatment, image analysis (WinROOF®) of Ti elemental mapping results were carried out (Fig. S4 and Table S2).

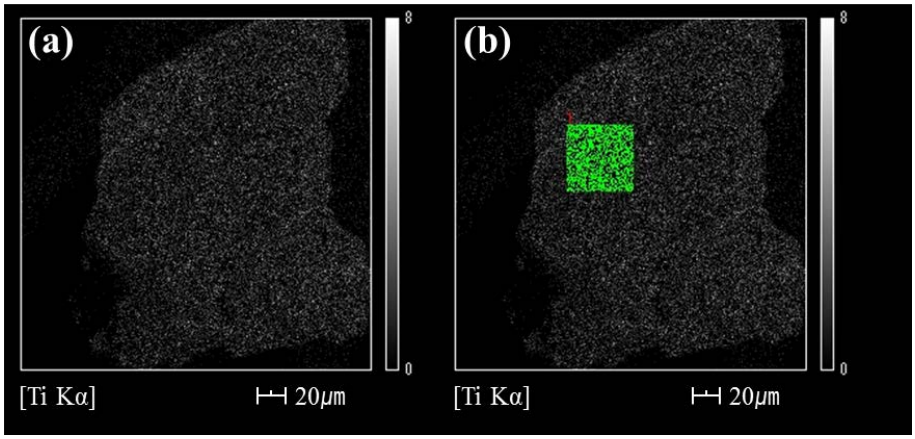


**Fig. S4.** A representative result of image analysis using WinROOF®. Areas in green are areas of Ti signals on arsenopyrite surface.

**Table S2.** Coating coverage on arsenopyrite of $TiO_2$ measured using image analysis.

| Image No. | Ti area (μm$^2$) | Total area (μm$^2$) | % of total |
|---|---|---|---|
| 1 | 533.3 | 920.2 | 58.0 |
| 2 | 530.0 | 877.4 | 60.4 |
| 3 | 555.8 | 913.6 | 60.8 |
| 4 | 578.9 | 1014.5 | 57.1 |
| 5 | 571.7 | 920.2 | 62.1 |
| 6 | 641.4 | 1012.3 | 63.4 |
| 7 | 424.7 | 873.0 | 48.6 |
| 8 | 568.4 | 967.4 | 58.8 |
| 9 | 547.6 | 913.6 | 59.9 |
| 10 | 509.7 | 814.8 | 62.6 |
| Average | | | 59.2 ± 4.2 |